Laminar burning characteristics of 2-methylfuran and isooctane blend fuels

Xiao Ma [a], Changzhao Jiang [a], Hongming Xu [a,b,*], Haichun Ding [a], Shijin Shuai [b]

[a] School of Mechanical Engineering, University of Birmingham, Birmingham B15 2TT, UK
[b] State Key Laboratory of Automotive Safety and Energy, Tsinghua University, Beijing 100084, China

HIGHLIGHTS

- We studied laminar burning characteristics of MF–isooctane blended fuels.
- The highest un-stretched flame speeds occur in a range of Φ 1.1–1.2.
- Markstein number and burning velocities of MF20 and MF50 are presented.
- MF fraction has larger effects on burning velocities at higher temperatures.

ARTICLE INFO

ABSTRACT

2-Methylfuran (MF) has become very attractive due to the recent breakthrough in its production method using the process of dehydration and hydrogenolysis of fructose. MF–gasoline blended fuel has been considered as a potential choice of alternative fuel pathway for spark ignition (SI) engines, as have other bio-fuel blends. Isooctane is used to represent gasoline in fundamental studies of gasoline blended fuels, however, little is known about the laminar burning characteristics of MF–isooctane blended fuels. In this study, high-speed schlieren photography is used to investigate the laminar burning characteristics of gaseous MF–isooctane at varying temperatures and equivalence ratios with an initial pressure of 0.1 MPa in a constant-volume vessel. The outwardly spherical flame method is used to determine the stretched flame speeds. The un-stretched flame speeds, Markstein lengths, Markstein number, laminar burning velocities and laminar burning flux of MF20 (20% MF and 80% isooctane) and MF50 (50% MF and 50% isooctane) under different equivalence ratios and temperatures are then deduced and compared to MF and isooctane. The results show that the un-stretched flame speeds and laminar burning velocities of MF20 and MF50 are between those of MF and isooctane under all conditions. The peak un-stretched flame speeds of the blends occur in an equivalence ratio range of 1.1–1.2 at all temperatures, closer to the case of MF at higher temperatures. Both blended fuels have Markstein lengths closer to isooctane at an equivalence ratio lower than 1.2 at all temperatures. The burning velocities of MF50 are very close to the average values for MF and isooctane, particularly at 393 K. MF in the blended fuel presents larger effects on burning velocities at higher temperatures.

© 2013 Elsevier Ltd. All rights reserved.

1. Introduction

Alternative bio-fuels present a potential pathway to provide sustainable–renewable sources and address the challenging issues of fossil fuel depletion and global warming. Previous research on alternative fuels has been wide ranging [1–3] and fuels that can be produced from celluloses have been considered as the most promising candidates. Ethanol has been thought of as the market-leading gasoline alternative [4–6] due to its mature mass

production methods [7,8]. However, a new production method for furan-type fuels has been developed in recent years [9] since high efficiency was achieved in producing 2,5-dimethylfuran (DMF) and 2-methylfuran (MF) from celluloses, indicating the prospect of industrial mass production [9–11]. MF and DMF have become quite attractive in alternate fuel studies because of their similarities to gasoline.

Table 1 shows the properties of MF and gasoline [12,13]. The properties of isooctane are also presented here because isooctane has been used as a representative component for gasoline in many studies [14].

The authors' group has studied previously the combustion and emissions of DMF and MF in a direct-injection spark-ignition (DISI)

Table 1
Properties of the test fuels compared to gasoline and DMF [12,13].

|	MF	DMF	Isooctane	Gasoline
Chemical formula				C2–C14
H/C ratio	1.2	1.333	2.25	1.795
O/C ratio	0.2	0.167	0	0
Gravimetric oxygen content (%)	19.51	16.67	0	0
Density @ 20 C (kg/m^3)	913.2	889.7	691.9	744.6
Research Octane Number (RON)	103	101.3	100	96.8
Motor Octane Number (MON)	86	88.1	100	85.7
Stoichiometric air–fuel ratio	10.05	10.72	15.13	14.46
LHV (MJ/kg)	31.2	32.89	44.3	42.9
LHV (MJ/L)	28.5	29.3	30.66	31.9
Heat of vaporization (kJ/kg)	358.4	332	307.63	373
Initial boiling point (_C)	64.7	92	99	32.8
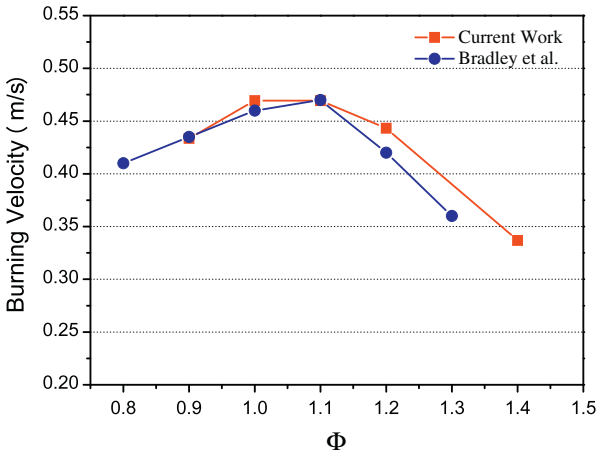
Fig. 3. Comparison of the laminar burning velocities from the current work and other researcher's results (isooctane, near 363 K) [40].
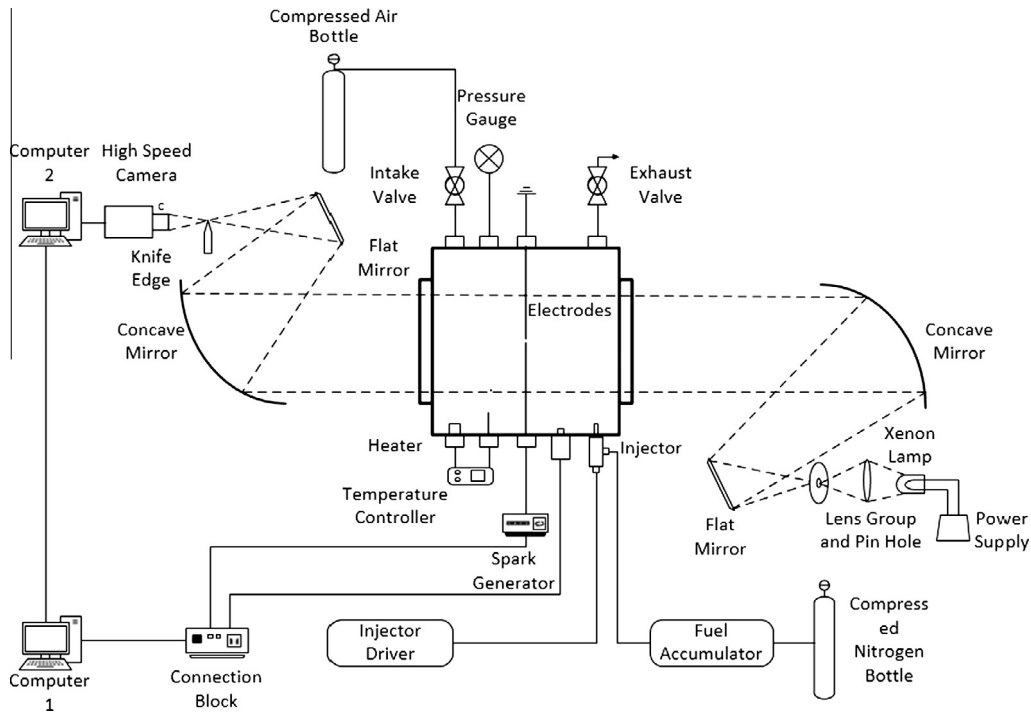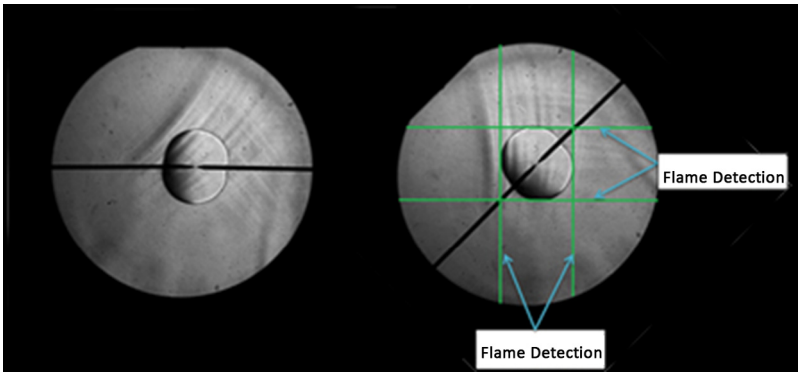
Fig. 1. Schlieren experimental setup.

Fig. 2. Laminar flame radius detection (left: original; right: rotated).

single-cylinder engine [15–17]. The results show that DMF can produce combustion and emission qualities competitive with gasoline and MF has more significant advantages when it is applied in a DISI engine. It has been revealed that the combustion of MF is faster than that of DMF and gasoline, which is good for knock suppression, and the PM emissions of MF are lower than those of gasoline in DI mode because of the molecular oxygen content. Similar results can also be found in the work of Thewes et al. [18].

Mixing an alternative fuel with gasoline is a realistic choice for the application of an alternative fuel, because current engine designs and configurations need fewer changes than would be needed to re-optimize their fuel supply systems for a pure alternative fuel. Meanwhile, low-percentage blending may also reduce the costs for modifying fuel production, transportation and storage/sale systems for the new fuels, which are critical issues to the commercial market. Much work has been done in alternative-blended fuel studies [19–21]. Rothamer and Jennings [22] compared the knocking propensity of DMF–gasoline blends with that of ethanol–gasoline blends. The results indicated that a blend with 10% DMF provided the best performance in fuel consumption. Wu
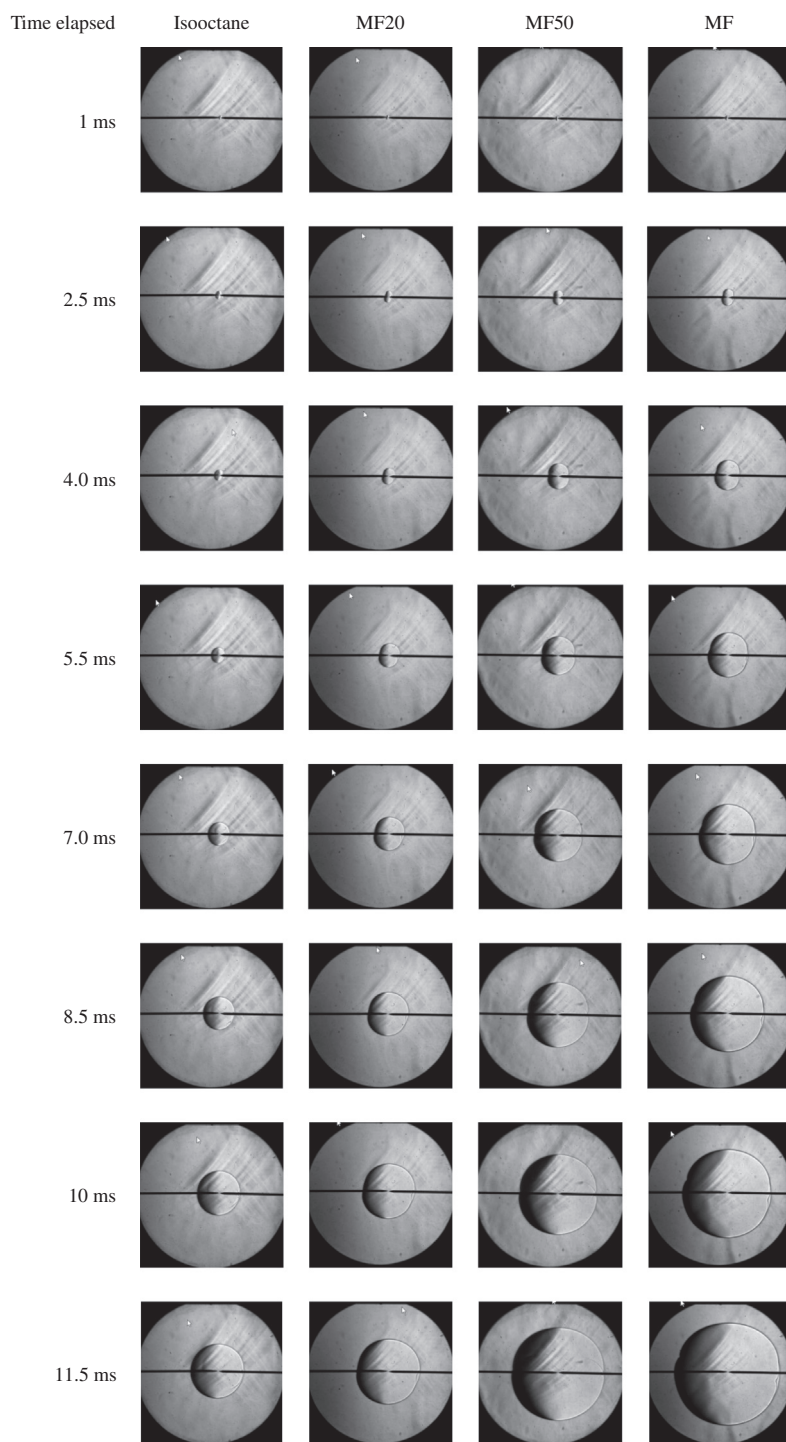

Fig. 4. Chronological schlieren images of stoichiometric fuel–air mixtures at an initial temperature of 363 K.

et al. [23–25] studied the laminar flame propagation characteristics of DMF–isooctane blends at elevated pressures and temperatures and their further application in a DISI engine.

Laminar flame propagation characteristics are important fundamental physicochemical properties of a fuel–air mixture for validating the chemical reaction mechanisms and gaining a better understanding of the combustion process in engines [26,27]. Little is known about the laminar flame propagation characteristics of MF and MF blended fuels. In the present paper, the schlieren photography method was used to investigate the laminar flame speed, Markstein length, Markstein number, laminar burning velocity and burning flux. This has followed our work on the similar measurement of DMF-air mixtures at elevated temperatures in a wide range of equivalence ratios compared with ethanol and gasoline [28]. As gasoline, a compound of many species, is too complex for detailed chemical reaction mechanism analyses, isooctane was used in this study as a representative component of gasoline, similarly to previous works [12,29–31].

2. Experimental setup

Fig. 1 shows the schlieren system used in this study. A constant-volume vessel with two circular quartz windows (100 mm in diameter) on opposite sides, and eight heating units, one in each corner, was used for the experiment. The air–fuel mixture was heated by closed-loop controlled heating units. A gasoline direct injection (GDI) nozzle was mounted in the top cover of the vessel for fuel injection, which was driven by an ECU-computer system. A pair of electrodes was installed on two sides of the vessel. A high-voltage unit was used to supply the power for generating sparks between the electrodes.

A 500-W xenon lamp was coupled with a lens group, and a pinhole was used to generate a point light source for the schlieren test. A concave mirror produced parallel light which passed through the test field in the vessel. After being reflected by a second concave mirror, the light was then cut by a knife edge at the focus for the schlieren effect. A Phantom V710 high-speed camera was synchronized with the spark timing to record the image sequences at a sampling rate of 10,000 fps and a resolution of 800 × 800 pixels.

Compressed air was used to scavenge the burned gases in the exhaust. After flushing and before each test, the vessel chamber was opened to the ambient air until the air temperature inside the vessel stabilized at the test point. Fuels were injected into the chamber after the vessel was sealed. Then the chamber was left undisturbed for 5 min to ensure the homogeneousness and quiescence of the mixtures. Finally, the mixtures were ignited by a triggered electrode discharge, and the camera was triggered at the same time.

The tests were performed at initial temperatures of 333 K, 363 K and 393 K, with an initial pressure of 0.1 MPa. The equivalence ratios varied from 0.8 or 0.9 to 1.4. Each point of the tests was repeated at least three times.
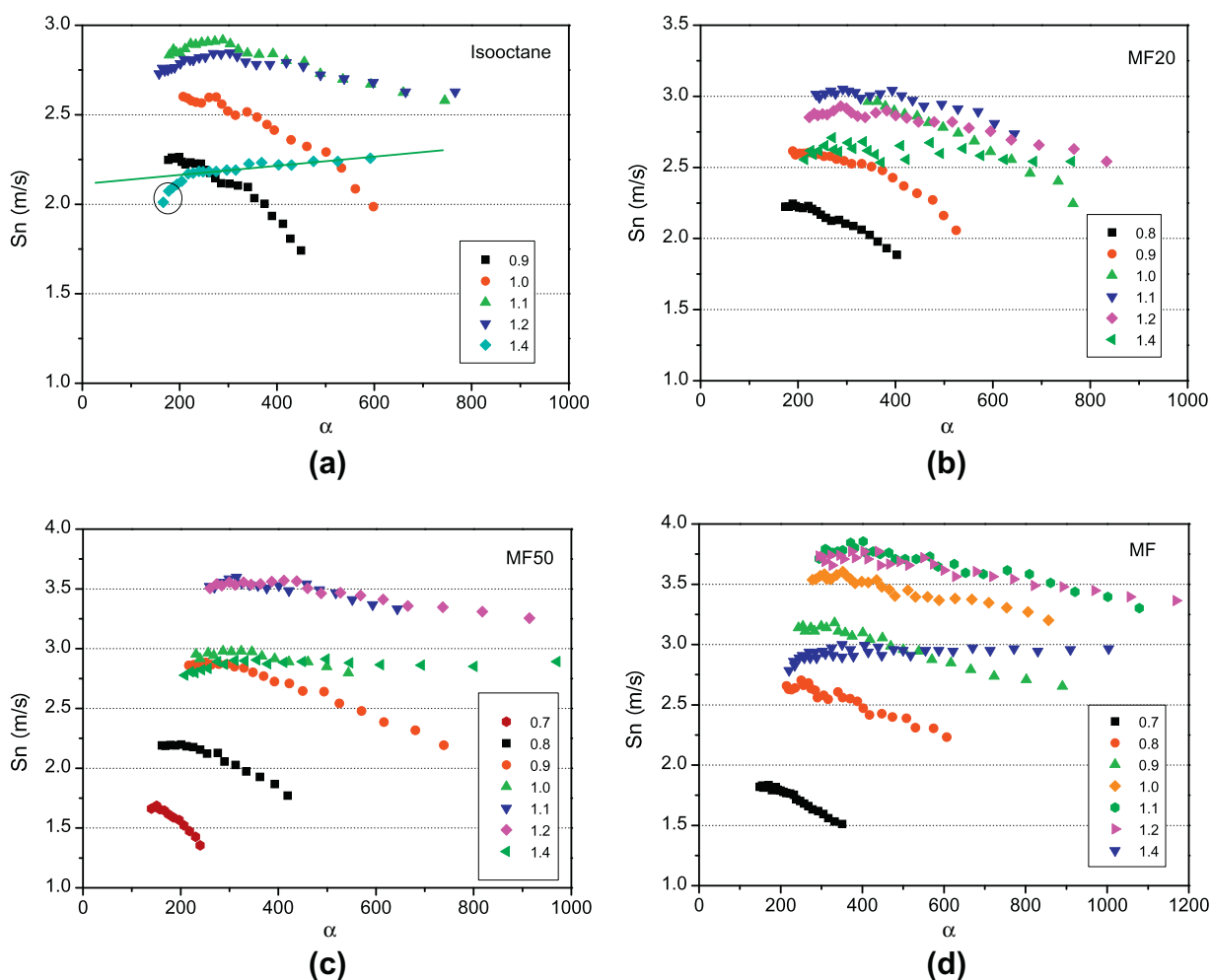

Fig. 5. Stretched flame speed of the test fuels at 363 K initial temperature with different equivalence ratios and stretch rates (a) isooctane, (b) MF20, (c) MF50 and (d) MF.

3. Image processing

The schlieren images were processed using an in-house-developed MATLAB code to determine the laminar flame characteristics as in the previous work [28]. The flame radii were measured in four directions at an included angle of 45° with the electrodes to reduce the effect of quenching near the surface. The flame fronts were identified by detecting the gradients in the grayscale images (see Fig. 2). All the results in the analysis were averaged from the three tests.

In order to avoid the effect of the spark ignition disturbance [32,33], the pressure increase resulting from the burning [34] and the space confinement [35], only images with flame radii of 6–25 mm were used. This range was validated as an optimized range with the current setup by previous study [28]. The stretched laminar flame speed S_n was determined by using the following equation:

$$S_n = dr_u/dt, \tag{1}$$

where r_u is the flame radius and t is the time after ignition. By knowing the stretched laminar flame speed, the stretch rate, α, is calculated by [36,37]:

$$\alpha = 2S_n/r_u, \tag{2}$$

The linear correlations between the stretch rate and flame speed are expressed by [36,37]:

$$S_n = S_L - L_b \times \alpha, \tag{3}$$

where S_L is laminar flame speed and L_b is Markstein length. S_L is determined by extrapolating S_n to a zero stretch rate. L_b is the negative value of the gradient of the flame propagation speed against the stretch rate curve.

The laminar burning velocity (μ_l) can be obtained from the equation [36,37]:

$$\mu_l = S_s \times \rho_b/\rho_u, \tag{4}$$

where ρ_b and ρ_u are the burned and unburned mixture densities, respectively. Assuming the pressure is constant, the burned (ρ_b) and unburned gas densities (ρ_u) can be found from the conservation of mass equation:

$$\rho_b/\rho_u = V_u/V_b = n_u T_u/n_b T_b, \tag{5}$$

where n_u and n_b are the number of moles of reactants and products, and T_u and T_b are the initial and adiabatic flame temperatures.

The density ratio is defined as:

$$\delta = \rho_u/\rho_b, \tag{6}$$

The adiabatic flame temperatures were calculated using HPFLAME [38], which incorporates the Olikara and Borman equilibrium routines [39].

The flame thickness is calculated by the ratio of kinematic viscosity to laminar flame velocity via [24,25]:
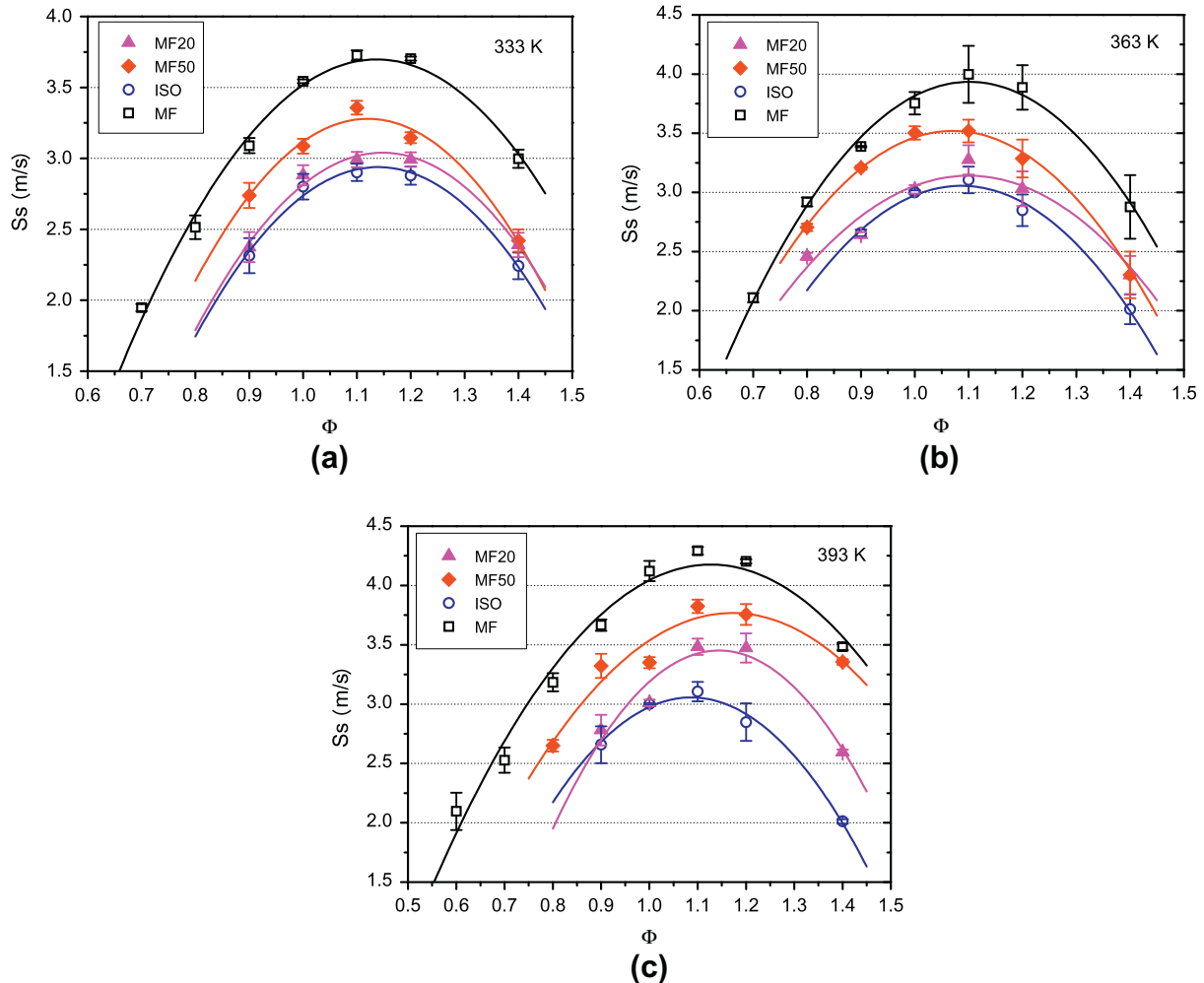
$$\delta_l = \nu/\mu_l. \tag{7}$$

Fig. 6. Un-stretched flame speed of the test fuels at different temperatures and equivalence ratios (a) 333 K, (b) 363 K and (c) 393 K.

The Markstein number is calculated from Markstein length and the flame thickness [36]:

$$M_a = L_b/\delta_l \tag{8}$$

The laminar burning flux, which reveals the eigenvalue of the flame propagation, is calculated by [36]:

$$f = \mu_l \times \rho_u. \tag{9}$$

4. Results and discussion

4.1. System validation

In order to validate the current measurement data, the obtained isooctane burning velocities at different equivalence ratios are compared with the data from previous studies in the literature. Fig. 3 shows that the results at 363 K in the current work agree well with the data from Bradley et al. [40] which were obtained under similar conditions. The differences at high equivalence ratios may be attributed to the different methods [25,41].

4.2. Flame morphology

Fig. 4 shows the schlieren images of four fuels at stoichiometric conditions with an initial temperature of 363 K and an initial pressure of 0.1 MPa. The flame propagation speeds of MF20 and MF50

are between those of MF and isooctane. When the flame approaches the vessel wall, the shape of the flame becomes distorted with a flatter surface on the upper side due to the influence of the internal geometry [35]. Due to the quenching effect of the electrodes, all flame propagation speeds are slower along the direction of the electrodes than in the vertical direction; thus the flame is not perfectly spherical. The wrinkling near the electrodes is also attributed to the quenching effect. All the images for calculation were chosen such that significant large wrinkling on the flame front surface, which may affect the results, was avoided.

4.3. Flame propagation and Markstein length

4.3.1. Stretched flame propagation speed

The stretched flame propagation speed versus stretch rate (marked as α, in the figures) for the three fuels at different equivalence ratios under 393 K are shown in Fig. 5. As the flame expands in the vessel, the flame stretch rate reduces due to the inverse proportionality between the flame stretch rate and flame radius. The linear correlation between the flame stretch rate and the flame radius at a large stretch rate is considered as representative of the laminar flame characteristics [28]. However, in some cases, the non-linear trends also appear at a large stretch rate. For instance, in Fig. 5a and b, most of the results show a bending trend at maximum stretch rates. This is because of the unstable combustion at the stage shortly after ignition. In some lean-burn cases, e.g., the
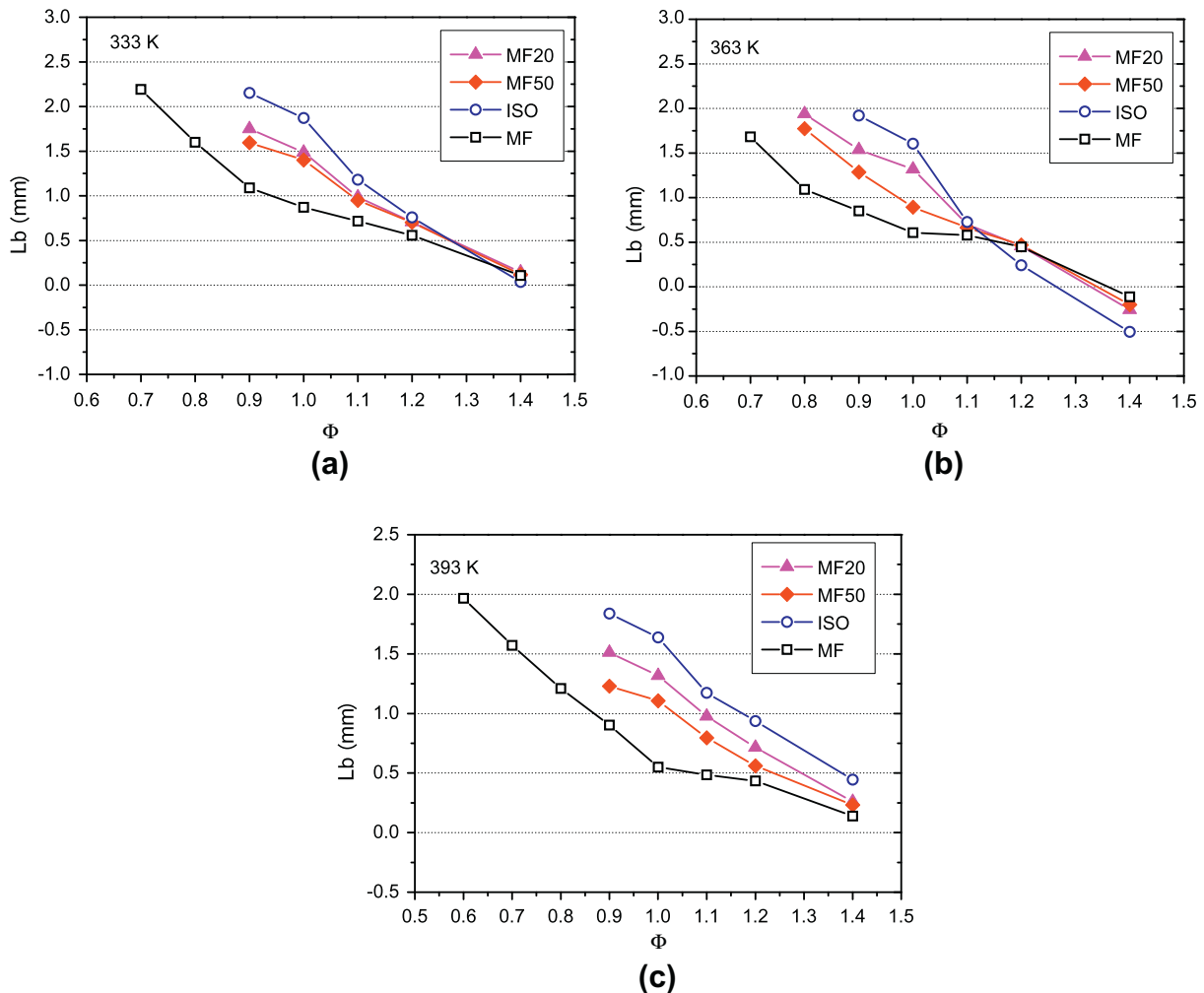

Fig. 7. Markstein length of test fuels at different temperatures and equivalence ratios (a) 333 K, (b) 363 K and (c) 393 K.

Φ = 0.9 case of isooctane, the problem appears more serious. In order to extract the un-stretched flame speed and Markstein length correctly, those points which are too far from the linear trend will be removed as bad data. The used points should give a deviation less than 5% for the fitting result, and the offset to the fitting line of the single points are also limited within 5%, while keeping as many data points as possible. Fig. 5ashows an example of dropping the bad data points in the fitting process and the circled points were removed for the fitting results.

4.3.2. Un-stretched flame propagation speed

Along with the stretched flame propagation speeds, the un-stretched flame propagation speeds and the Markstein length were obtained by extrapolating the un-stretched flame propagation speeds to a zero stretch rate ($\alpha = 0$) and calculating the gradient of the stretched flame propagation speed using the stretch rate slope in the linear range, respectively. Fig. 6 reveals the un-stretched flame speeds of the four fuels at different temperatures and equivalence ratios. The scattering points indicate the experimental results, and the solid lines are quadratic fit curves. For all temperatures (333 K, 363 K and 393 K), MF has the highest un-stretched flame propagation speeds at all the equivalence ratios, while isooctane has the lowest. The results of the two blend fuels are between those of the pure fuels as expected. In all the cases, the peak un-stretched flame speeds appear around an equivalence

ratio of 1.1–1.2. Higher temperature leads to a larger difference between MF and isooctane. It is notable that the differences between MF20 and isooctane also increase when the temperature increases. For instance, at 333 K and under most equivalence ratios, the un-stretched flame propagation speeds of MF20 are about 0.1 m/s faster than those of isooctane, while the differences increase to about 0.5 m/s at 393 K. The results for MF50 are generally in the middle of MF and isooctane.

4.3.3. Markstein length, flame thickness and Markstein number

The Markstein length indicates the influence of stretch rate on flame propagation speed, which characterizes the diffusion-thermal instability [26,42]. The asymptotic theory [43] points out that the Markstein length depends on the Lewis number of the fuel for a lean mixture, or that of oxidizer for a rich mixture. Normally, the Markstein length decreases with an increase of equivalence ratio for heavy hydrocarbon–air mixtures, while the trend is opposite for light hydrocarbon–air mixtures [44].

Fig. 7 shows the Markstein lengths of the four fuels at different temperatures and equivalence ratios. The Markstein lengths decrease with an increase of equivalence ratio as a trend, which is consistent with the theory as in [44] since both MF and isooctane have more than five carbon or/and oxygen atoms per molecule.

The Markstein lengths of MF are significantly smaller than those of isooctane at equivalence ratios lower than 1.0, while the
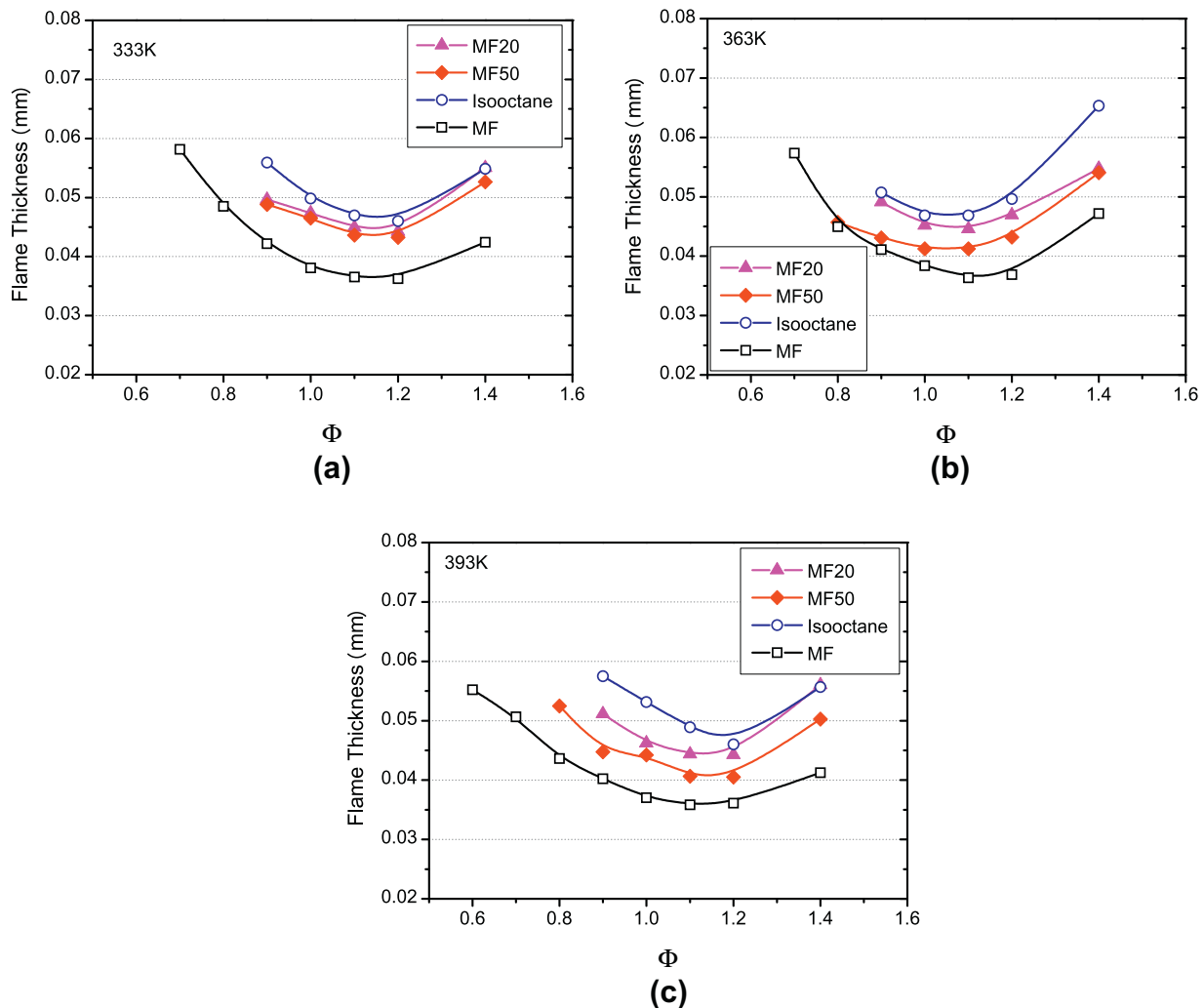

Fig. 8. Flame thickness of the test fuels at different temperatures and equivalence ratios (a) 333 K, (b) 363 K and (c) 393 K.

differences between them are much smaller at equivalence ratios higher than 1.0. The data for the two blended fuels are between those for the pure fuels at equivalence ratios below 1.2; both are however closer to the data of isooctane indicating its dominating role here. Positive Markstein lengths indicate that the flame speed decreases with an increase in the stretch rate, while a negative Markstein length indicates that the flame speed increases with an increase in the stretch rate. Thus in the range of equivalence ratios below 1.2, all the fuels have lower flame speeds when the stretch rate increases. Bradley et al. [40] pointed out that if the Markstein length is larger than 1.5, the flame will be initially stable until a critical flame radius is reached. This means isooctane and the two blended fuels have better initial flame stabilities than MF in a lean burning condition.

With respect to temperature, the differences between the Markstein lengths of MF at 363 K and 393 K with the same equivalence ratios are quite small; while the Markstein lengths of MF at 333 K are larger than those at the other two temperatures with low equivalence ratios (0.7–1.0). Negative values of the Markstein length under 393 K appear at rich equivalence ratios and this indicates that the MF flame is more unstable at these temperatures under rich conditions. Correspondingly, MF20 and MF50 also have similar trends. There is no significant difference between the two blended fuels under most conditions, and the temperature has no significant effect on the trends of the blended fuels.

Previous theory [26,45] indicates that there are mainly two kinds of flame surface instabilities acting on the flame front in conditions similar to those in the current work: the diffusion-thermal instability and the hydrodynamic instability. The diffusion-thermal instability is characterized by the Markstein length. The hydrodynamic instability, which is induced by the density transition across the flame front, is characterized by the flame thickness and the density ratio. A decrease in the flame thickness indicates the promotion of this kind of instability.

Fig. 8 shows flame thickness versus equivalence ratio for all of the test fuels at different initial temperatures. The trends revealed by the data are generally the same, showing a range of lower flame thickness near an equivalence ratio of 1.0, which indicates higher instability. Isooctane and MF have the highest and lowest values, respectively. The results of MF20 and MF50 are between those of the two pure fuels. For all four fuels, the flame thickness data is not sensitive to the variation of initial temperature except for some points at the lean and rich ends. This means the initial temperature is not the most important parameter affecting flame thickness in the test range, and thus the Markstein number is mainly determined by the Markstein length for the same fuel.

The Markstein number, which characterizes the effect of local heat release on the flame morphology and the flame front curvature, quantifies the response of a laminar flame to stretch and can be used to indicate the stability of laminar and turbulent flame fronts. Fig. 9 gives the values of the Markstein number at different
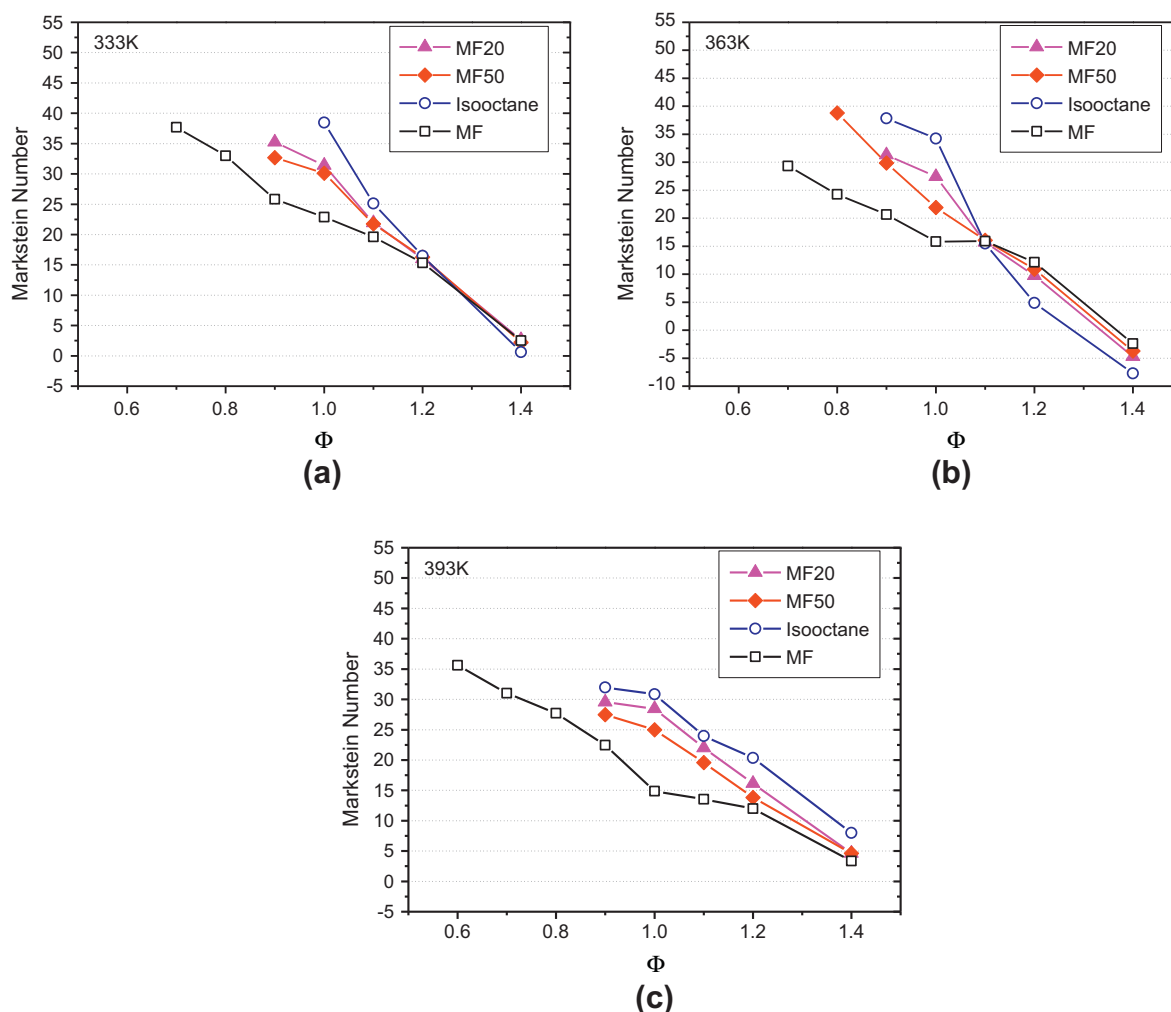

Fig. 9. Markstein number of the test fuels at different temperatures and equivalence ratios (a) 333 K, (b) 363 K and (c) 393 K.

initial temperatures. The Markstein numbers are generally decreasing with an increase in equivalence ratios, similar to the Markstein lengths. It is shown that the results of MF20 and MF50 are between those of the two pure fuels at most equivalence ratios and are closer to isooctane. Generally, the ranking of the fuels in terms of Markstein number for a given equivalence ratio does not change with temperature, except that some points at high equivalence ratios are very close. A cross-over point appears at equivalence ratio 1.1 under the initial temperature of 363 K, as shown in Fig. 9b, which also proves that the Markstein numbers of blended fuels depends on those of the pure fuels. The effect of temperature on the Markstein length for different fuels cannot be represented by a simple tendency [28], nor can the results for the Markstein number. The instability at high equivalence ratios may also result in larger errors. Therefore, it is quite difficult to discuss the ranking of fuels under different initial temperatures at a given equivalence ratio. More investigations are needed to provide a more detailed explanation in future studies.

4.4. Laminar burning velocities and burning flux

Laminar burning velocity is the speed at which the flame advances into the unburned mixture. Fig. 10 shows the laminar burning velocities at the equivalence ratios with different initial temperatures. The laminar burning velocities of MF, MF20 and MF50 under varying initial temperatures have peaks near the

equivalence ratio of 1.1, which is correlated to the state of the un-stretched flame speeds. Among all the fuels, MF has the highest laminar burning velocity under all conditions. The burning velocities of the two blended fuels are between those of the pure fuels, which is also similar to the trend shown by the un-stretched flame speeds. The burning velocities of MF50 near the equivalence ratio of 1.1 are quite close to the average values of MF and isooctane. Particularly for the cases at 393 K, the values for MF50 are close to the average values of MF and isooctane at all tested equivalence ratios.

Previous studies have pointed out that the laminar burning velocity is strongly related to the equivalence ratio and initial temperature of the reactants [46–48]. In Fig. 10 the laminar burning velocities for all the fuels increase when the initial temperature increases. For MF20 and MF50, the laminar burning velocities near the peaks at 393 K are about 0.05–0.07 m/s faster than the results at 363 K, and about 0.15–0.18 m/s faster than the results at 333 K. At higher equivalence ratios, the differences between blended fuels are smaller at 333 K, and the laminar burning velocities of the blended fuel are closer to those of isooctane, whereas at 393 K, no such phenomena are observed. This means MF has a greater effect in determining the laminar burning velocity in blended fuels at higher initial temperatures. As mentioned in a previous section, the work of Wang et al. [17] found the combustion duration of MF is significantly shorter than that of gasoline in a DISI engine. The burning velocity data here clearly proves the conclusion that MF
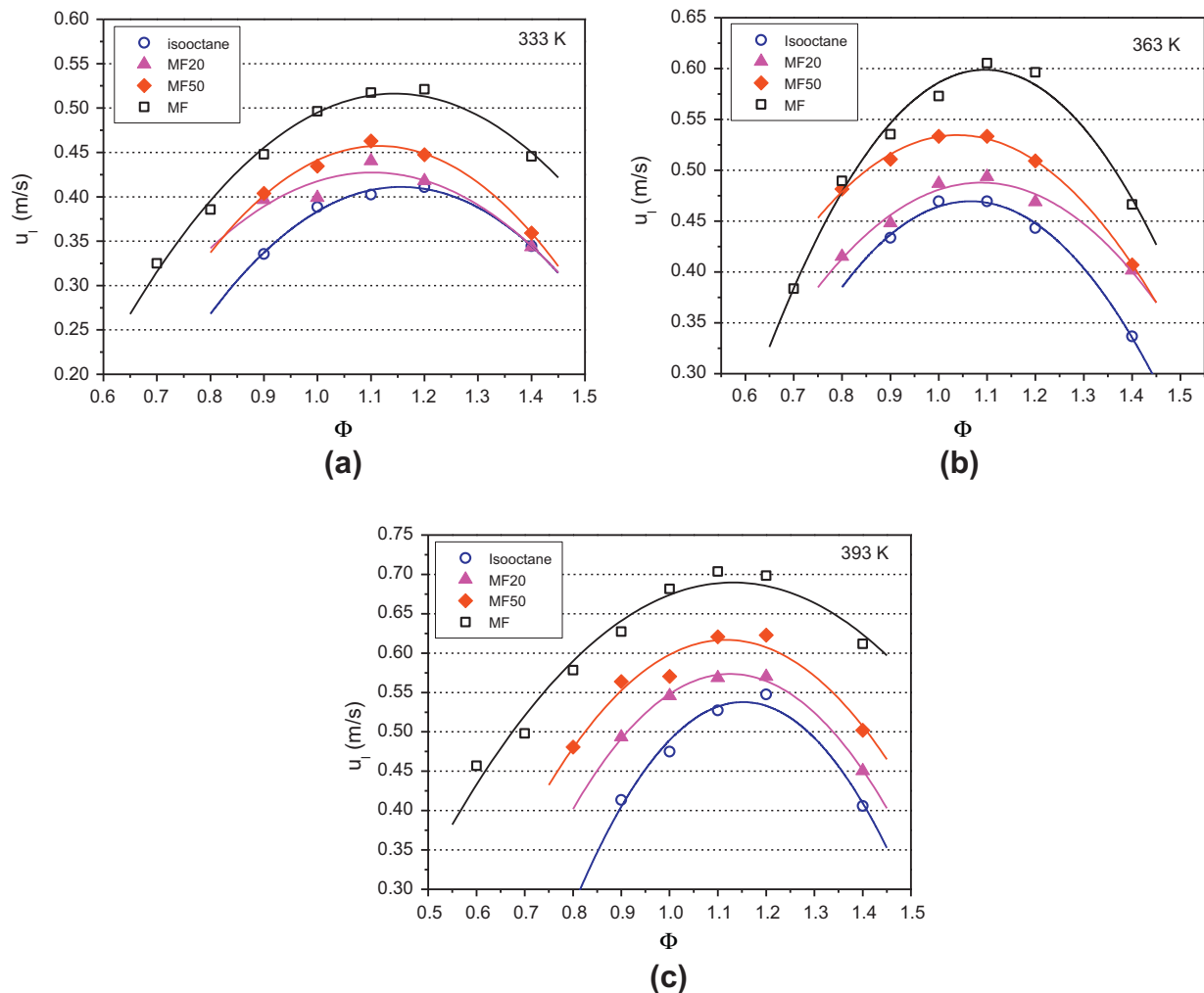

Fig. 10. Laminar burning velocities of test fuels at different temperatures and equivalence ratios (a) 333 K, (b) 363 K and (c) 393 K.
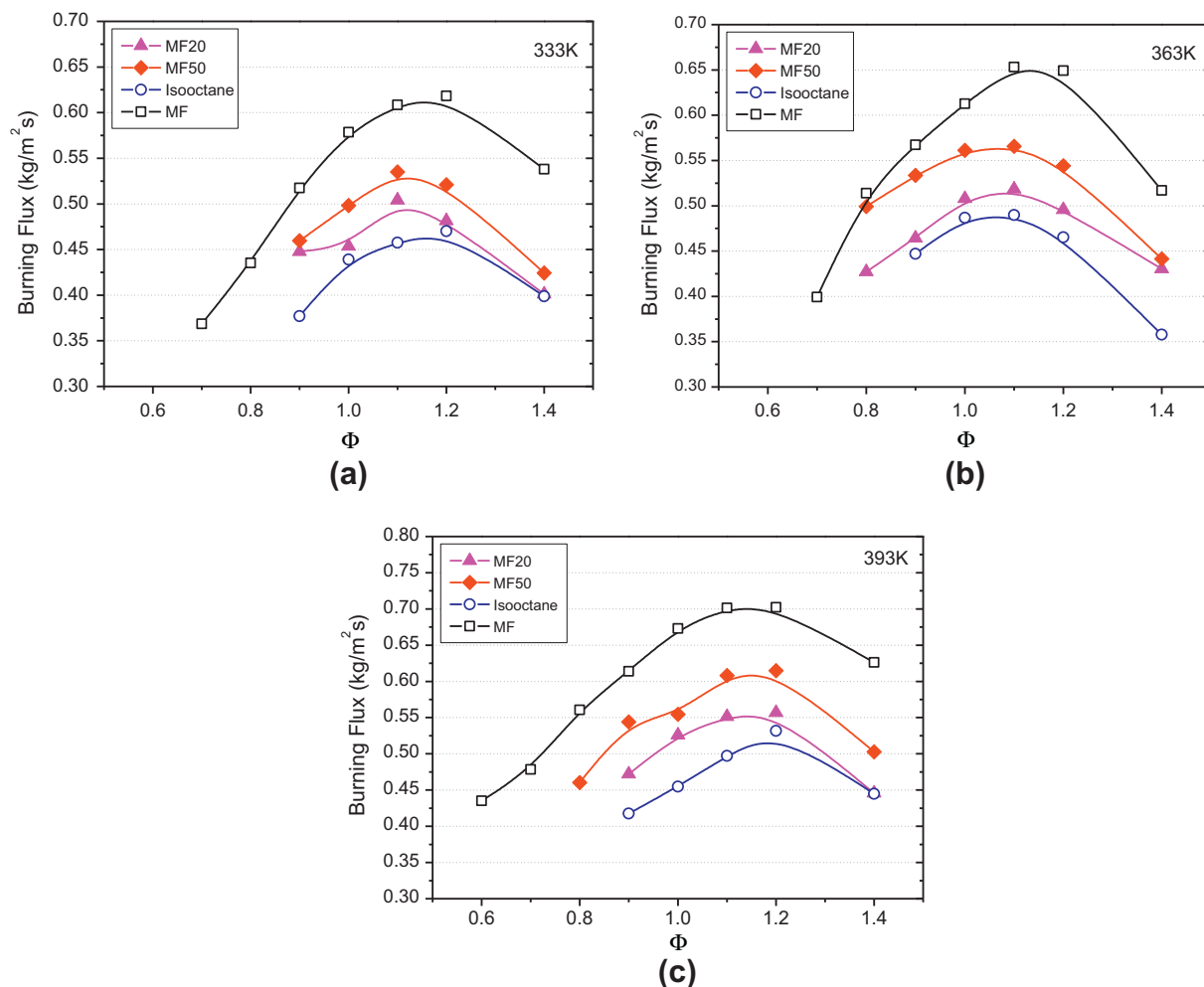
Fig. 11. Burning flux of test fuels at different temperatures and equivalence ratios (a) 333 K, (b) 363 K and (c) 393 K.

has faster combustion; which results in a higher indicated thermal efficiency than gasoline. At high temperatures, MF in the blended fuels significantly promotes the burning velocity because of its high chemical activity. This offers fundamental support to improving performance by adding MF to SI engine fuel.

Fig. 11 shows the burning flux versus equivalence ratio for MF at different initial temperatures. At each temperature and equivalence ratio, laminar burning flux is in the order of MF, MF50, MF20 and isooctane from the highest to the lowest value, corresponding to the order of the burning velocities. The peak values of the burning flux of all the fuels at three temperatures appear between equivalence ratios of 1.0 and 1.2. With respect to temperature, the burning flux of all the fuels increases with an increase in the initial temperature. The burning flux of the two blended fuels varies in a range of 0.45–0.62 near the stoichiometric state at all the initial temperatures.

5. Conclusions

In this study, the laminar combustion characteristics of 2-methylfuran (MF) and MF–isooctane blended fuels was investigated using high-speed schlieren photography at elevated temperatures (333 K, 363 K and 393 K) and varying equivalence ratios ($\Phi = 0.7$–1.4) under 0.1 MPa initial pressure in a constant volume vessel. The characteristics of the blended fuels were compared to

the cases of MF and isooctane. The following conclusions are drawn from the results:

1. The un-stretched flame speeds of MF20 and MF50 are between those of MF and isooctane under all the tested conditions. The highest un-stretched flame speeds of all four fuels occur in an equivalence ratio range of 1.1–1.2 at all tested temperatures. The peak un-stretched flame speeds of the blended fuels are closer to the data of MF at higher temperatures.
2. The blended fuel flames are less stable than isooctane's flame but more stable than MF's flame at equivalence ratios lower than 1.0 at all the tested temperatures. The difference between the flames of MF20 and MF50 is not significant. The Markstein numbers show similar trends as the Markstein lengths. Both blended fuels have the Markstein number closer to that of isooctane at equivalence ratios lower than 1.2.
3. The laminar burning velocities of the blended fuels are between those of MF and isooctane. The data of MF50 is close to the average data of MF and isooctane, particularly at 393 K. The laminar burning velocities near the peaks of the blended fuels at 393 K is about 0.05–0.07 m/s faster than the results at 363 K and about 0.15–0.18 m/s faster than the results at 333 K. The burning flux of the two blended fuels varies in a range of 0.45–0.62 near the stoichiometric state at all the tested initial temperatures.

Acknowledgments

The present work is part of a three-year research project sponsored by the Engineering and Physical Sciences Research Council (EPSRC) under Grant EP/F061692/1. The authors wish to especially thank Professor C.K Law of Princeton University for his advice and discussion on the work.

References

[1] Stein R, Polovina D, Roth K, Foster M, et al. Effect of heat of vaporization, chemical octane, and sensitivity on knock limit for ethanol–gasoline blends. SAE Int J Fuels Lubr 2012;5(2):823–43.
[2] Kale V, Santoso H, Marriott C, Worm J, et al. Combustion robustness characterization of gasoline and E85 for startability in a direct injection spark-ignition engine. SAE Technical Paper 2012-01-1073; 2012.
[3] Merola S, Marchitto L, Corcione F, Valentino G, et al. Optical diagnostics of the pollutant formation in a CI engine operating with diesel fuel blends. SAE Int J Engines 2011;4(2):2543–58.
[4] U.S. Department of Energy. US Ethanol Industry: the next inflection point. B Curtis Energies and Resource Group, 2007 year in review; 2008.
[5] Goldemberg J. The challenge of biofuels. Energy Environ Sci 2008;1:523–5.
[6] Demirbas A. Progress and recent trends in biofuels. Prog Energy Combust Sci 2007;33:1–18.
[7] Agarwal AK. Biofuels (alcohols and biodiesel) applications as fuels for internal combustion engines. Prog Energy Combust Sci 2007;33(3):233–71.
[8] Rakopoulos DC, Papagiannakis RG, Kyritsis DC. Combustion heat release analysis of ethanol or n-butanol diesel fuel blends in heavy-duty DI diesel engine. Fuel 2011;90:1855–67.
[9] Roman-Leshkov R, Barrett CJ, Liu ZY, Dumesic JA. Production of dimethylfuran for liquid fuels from biomass-derived carbohydrates. Nature 2007;447:982–6.
[10] Luque R, Herrero-Davila L, Campelo JM, et al. Biofuels: a technological perspective. Energy Environ Sci 2008;1:542–64.
[11] Zhao H, Holladay JE, Brown H, Zhang ZC. Metal chlorides in ionic liquid solvents convert sugars to 5-hydroxymethylfurfural. Science 2007;316:1597–600.
[12] Janet Y, Earl C, McCormick R. Utilization of renewable oxygenates as gasoline blending components. National Renewable Energy Laboratory; 2011.
[13] Heywood JB. Internal combustion engine fundamental. McGraw-Hill Book Company; 1989.
[14] Ma X, He X, Wang J, Shuai S. Co-evaporative multi-component fuel design for in-cylinder PLIF measurement and application in gasoline direct injection research. Appl Energy 2011;88(8):2617–27.
[15] Zhong S, Daniel R, Xu H, et al. Combustion and emissions of 2,5-dimethylfuran in a direct injection spark-ignition engine. Energy Fuels 2010;24(5):2891–9.
[16] Daniel R, Tian G, Xu H, Wyszynski ML, et al. Effect of spark timing and load on a DISI engine fuelled with 2,5-dimethylfuran. Fuel 2011;90(2):449–58.
[17] Wang C, Xu H, Daniel R, et al. Combustion characteristics and emissions of 2-methylfuran compared to 2,5-dimethylfuran, gasoline and ethanol in a DISI engine. Fuel 2013;103:200–11.
[18] Thewes M, Muether M, Pischinger S, et al. Analysis of the impact of 2-methylfuran on mixture formation and combustion in a direct-injection spark-ignition engine. Energy Fuels 2011;25(12):5549–61.
[19] Price P, Twiney B, Stone R, Kar K, et al. Particulate and hydrocarbon emissions from a spray guided direct injection spark ignition engine with oxygenate fuel blends. SAE Technical Paper 2007-01-0472; 2007.
[20] Aleiferis P, Malcolm J, Todd A, Cairns A, et al. An optical study of spray development and combustion of ethanol, iso-octane and gasoline blends in a DISI engine. SAE Technical Paper 2008-01-0073; 2008.
[21] Broustail G, Seers P, Halter F, Moréac G, et al. Experimental determination of laminar burning velocity for butanol and ethanol iso-octane blends. Fuel 2011;90(1):1–6.
[22] Rothamer D, Jennings J. Study of the knocking propensity of 2,5-dimethylfuran–gasoline and ethanol–gasoline blends. Fuel 2012;98:203–12.
[23] Wu X, Daniel R, Tian G, Xu H, et al. Dual-injection: the flexible, bi-fuel concept for spark-ignition engines fuelled with various gasoline and biofuel blends. Appl Energy 2011;88:2305–14.
[24] Wu X, Huang Z, Wang X, et al. Laminar burning velocities and flame instabilities of 2,5-dimethylfuran–air mixtures at elevated pressures. Combust Flame 2011;158(3):539–46.
[25] Wu X, Li Q, Fu J, et al. Laminar burning characteristics of 2,5-dimethylfuran and iso-octane blend at elevated temperatures and pressures. Fuel 2012;95:234–40.
[26] Law CK, Sung CJ. Structure, aerodynamics, and geometry of premixed flamelets. Prog Energy Combust Sci 2000;26:459–505.
[27] Beeckmann J, Röhl O, Peters N. Experimental and numerical investigation of iso-octane, methanol and ethanol regarding laminar burning velocity at elevated pressure and temperature. SAE Technical Paper 2009-01-1774; 2009.
[28] Tian G, Daniel R, Li H, Xu H, et al. Laminar burning velocities of 2,5-dimethylfuran compared with ethanol and gasoline. Energy Fuels 2010;24(7):3898–905.
[29] Serras-Pereira J, Aleiferis P, Richardson D, Wallace S. Characteristics of ethanol, butanol, iso-octane and gasoline sprays and combustion from a multi-hole injector in a DISI engine. SAE Int J Fuels Lubr 2009;1(1):893–909.
[30] Schulz C, Sick V. Tracer-LIF diagnostics: quantitative measurement of fuel concentration, temperature and fuel/air ratio in practical combustion systems. Prog Energy Combust Sci 2005;31(1):75–121.
[31] Broustail G, Halter F, Seers P, et al. Comparison of regulated and non-regulated pollutants with iso-octane/butanol and iso-octane/ethanol blends in a port-fuel injection spark-ignition engine. Fuel 2012;94:251–61.
[32] Chen Z, Burke MP, Ju Y. Effects of Lewis number and ignition energy on the determination of laminar flame speed using propagating spherical flames. Proc Combust Inst 2009;32:1253–60.
[33] Huang Z, Zhang Y, Zeng K, Liu B, Wang Q, et al. Measurements of laminar burning velocities for natural gas–hydrogen–air mixtures. Combust Flame 2006;146:302–11.
[34] Zhang Z, Huang Z, Wang X, Xiang J, et al. Measurements of laminar burning velocities and Markstein lengths for methanol–air–nitrogen mixtures at elevated pressures and temperatures. Combust Flame 2008;155:358–68.
[35] Burke MP, Chen Z, Ju Y, Dryer FL. Effect of cylindrical confinement on the determination of laminar flame speeds using outwardly propagating flames. Combust Flame 2009;156:771–9.
[36] Bradley D, Hicks RA, Lawes M, Sheppard CGW, et al. The measurement of laminar burning velocities and Markstein numbers for iso-octane-air and iso-octane-n-heptane-air mixtures at elevated temperatures and pressures in an explosion bomb. Combust Flame 1998;115:126–44.
[37] Gu XJ, Haq MZ, Lawes M, Woolley R. Laminar burning velocity and Markstein lengths of methane–air mixtures. Combust Flame 2000;121:41–58.
[38] Turns SR. An introduction to combustion. New York: McGraw-Hill; 1996.
[39] Olikara C, Borman GL. A computer program for calculating properties of equilibrium combustion products with some applications to I.C. engines. SAE Technical Paper 750468; 1975.
[40] Bradley D, Hicks RA, Lawes M, Sheppard CGW, et al. The measurement of laminar burning velocities and Markstein numbers for iso-octane-air and isooctane isooctane-n-heptane-air mixtures at elevated temperatures and pressures in an explosion bomb. Combust Flame 1998;115:126–44.
[41] Hasse C, Bollig M, Peters N, et al. Quenching of laminar iso-octane flames at cold walls. Combust Flame 2000;122(1):117–29.
[42] Karlin V, Sivashinsky G. Asymptotic modelling of self-acceleration of spherical flames. Proc Combust Inst 2007;31:1023–30.
[43] Matalon M, Matkowsky BJ. Flames as gas dynamic discontinuities. J Fluid Mech 1982;24:239–59.
[44] Bechtold JK, Matalon M. The dependence of the Markstein length on stoichiometry. Combust Flame 2001;127:1906–13.
[45] Matalon M. Intrinsic flame instabilities in premixed and non-premixed combustion. Annu Rev Fluid Mech 2007;39:163–91.
[46] Stone Richard. Introduction to internal combustion engine. SAE International and Macmillan Press; 2012.
[47] Hirasawa T, Sung CJ, Joshi A, Yang Z, Wang H, Law CK. Determination of laminar flame speeds using digital particle image velocimetry: binary fuel blends of ethylene, n-Butane, and toluene. Proc Combust Inst 2002;29:1427–34.
[48] Tang CL, Huang ZH, Law CK. Determination, correlation, and mechanistic interpretation of effects of hydrogen addition on laminar flame speeds of hydrocarbon–air mixtures. Proc Combust Inst 2011;33:921–8.